ARTICLE

30. Kim, S. E., Coste, B., Chadha, A., Cook, B. & Patapoutian, A. The role of *Drosophila* piezo in mechanical nociception. *Nature* 19, 209–212 (2012).
31. Suzuki, S. *et al.* Differential roles of Epac in regulating cell death in neuronal and myocardial cells. *J. Biol. Chem.* 285, 24248–24259 (2010).
32. Akopian, A. N. *et al.* The tetrodotoxin-resistant sodium channel SNS has a specialized function in pain pathways. *Nat. Neurosci.* 2, 541–548 (1999).
33. Ostman, J. A., Nassar, M. A., Wood, J. N. & Baker, M. D. GTP up-regulated persistent Na + current and enhanced nociceptor excitability require NaV1.9. *J. Physiol.* 586, 1077–1087 (2008).
34. Minett, M. S. *et al.* Distinct Nav1.7-dependent pain sensations require different sets of sensory and sympathetic neurons. *Nat. Commun* 24, 791 (2012).
35. Hargreaves, K., Dubner, R., Brown, F., Flores, C. & Joris, J. A new and sensitive method for measuring thermal nociception in cutaneous hyperalgesia. *Pain* 32, 77–88 (1988).
36. Chaplan, S. R., Bach, F. W., Pogrel, J. W., Chung, J. M. & Yaksh, T. L. Quantitative assessment of tactile allodynia in the rat paw. *J. Neurosci. Methods* 53, 55–63 (1994).
37. Minett, M. S. *et al.* Distinct Nav1.7-dependent pain sensations require different sets of sensory and sympathetic neurons. *Nat. Commun.* 3, 791 (2012).
38. Lai, J. *et al.* Immunofluorescence analysis of antisense oligodeoxynucleotide-mediated 'knock-down' of the mouse delta opioid receptor *in vitro* and *in vivo*. *Neurosci. Lett.* 213, 205–208 (1996).
39. Hylden, J. L. & Wilcox, G. L. Intrathecal morphine in mice: a new technique. *Eur. J. Pharmacol.* 67, 313–316 (1980).
40. Mabuchi, T. *et al.* Pituitary adenylate cyclase-activating polypeptide is required for the development of spinal sensitization and induction of neuropathic pain. *J. Neurosci.* 24, 7283–7291 (2004).
41. Bennett, G. J. & Xie, Y. K. A peripheral mononeuropathy in rat that produces disorders of pain sensation like those seen in man. *Pain* 33, 87–107 (1988).
42. Dickenson, A. H. & Sullivan, A. F. Electrophysiological studies on the effects of intrathecal morphine on nociceptive neurones in the rat dorsal horn. *Pain* 24, 211–222 (1986).
43. Shpacovitch, V. M. *et al.* Agonists of proteinase-activated receptor-2 modulate human neutrophil cytokine secretion, expression of cell adhesion molecules, and migration within 3-D collagen lattices. *J. Leukoc. Biol.* 76, 388–398 (2004).
44. Gloerich, M. *et al.* Spatial regulation of cyclic AMP-Epac1 signaling in cell adhesion by ERM proteins. *Mol. Cell Biol.* 30, 5421–5431 (2010).
45. Cox, JJ. *et al.* An SCN9A channelopathy causes congenital inability to experience pain. *Nature* 444, 894–898.

Acknowledgements

Author contributions

Additional information

NATURAL PRODUCT COMMUNICATIONS

An International Journal for Communications and Reviews Covering all
Aspects of Natural Products Research

ANALYTICAL

SYNTHESIS

BIO-
TECHNOLOGY

BIODIVERSITY

BIOACTIVITY
& SAR

NPC

BIOSYNTHESIS

PHARMACO-
LOGY

MOLECULAR
STRUCTURE

CHEMICAL
ECOLOGY

INFORMATION FOR AUTHORS

Full details of how to submit a manuscript for publication in Natural Product Communications are given in Information for Authors on our Web site http://www.naturalproduct.us.

Authors may reproduce/republish portions of their published contribution without seeking permission from NPC, provided that any such republication is accompanied by an acknowledgment (original citation)-Reproduced by permission of Natural Product Communications. Any unauthorized reproduction, transmission or storage may result in either civil or criminal liability.

The publication of each of the articles contained herein is protected by copyright. Except as allowed under national "fair use" laws, copying is not permitted by any means or for any purpose, such as for distribution to any third party (whether by sale, loan, gift, or otherwise); as agent (express or implied) of any third party; for purposes of advertising or promotion; or to create collective or derivative works. Such permission requests, or other inquiries, should be addressed to the Natural Product Inc. (NPI). A photocopy license is available from the NPI for institutional subscribers that need to make multiple copies of single articles for internal study or research purposes.

To Subscribe: Natural Product Communications is a journal published monthly. 2012 subscription price: US$1,995 (Print, ISSN# 1934-578X); US$1,995 (Web edition, ISSN# 1555-9475); US$2,495 (Print + single site online); US$595 (Personal online). Orders should be addressed to Subscription Department, Natural Product Communications, Natural Product Inc., 7963 Anderson Park Lane, Westerville, Ohio 43081, USA. Subscriptions are renewed on an annual basis. Claims for nonreceipt of issues will be honored if made within three months of publication of the issue. All issues are dispatched by airmail throughout the world, excluding the USA and Canada.

Stereoselective Synthesis of Bicyclo[3.1.1]heptane Derivatives via Intramolecular Photocycloaddition Reaction

Kiyoshi Honda*, Mari Konishi, Manabu Kawai, Akihisa Yamada, Yasuhiko Takahashi, Yujiro Hoshino and Seiichi Inoue

Graduate School of Environment and Information Sciences, Yokohama National University,
Tokiwadai 79-5, Hodogaya-ku, Yokohama 240-8501, Japan
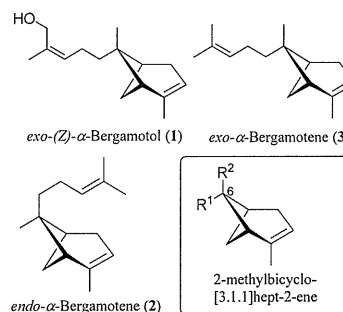
k-honda@ynu.ac.jp

Optically active 1,3-bridged cyclobutanes 10 of the bicyclo[3.1.1]heptane ring system and 1,2-bridged cyclobutanes 11 of the bicyclo[3.2.0]heptane ring system were produced by UV irradiation of $\alpha,\beta,\gamma,\delta$-unsaturated esters 9a and 9c-f. The preference of *endo*-stereochemistry at C-6 bridged head was observed in *cross*-adducts 10. On the other hand, irradiation of conjugated dienol9b led via only parallel cycloaddition to 1,2-bridged cyclobutane 11.

Keywords: Bicyclo[3.1.1]heptane ring system, Photocycloaddition, Synthesis of optically active 1,3-bridged cyclobutanes.

East Indian sandalwood oil contains some 4 to 8% of (−)-*exo*-(*Z*)-α-bergamotol ((−)-1), which has bright, somewhat sweet woo dy fragrance, and is consid ered to b e responsible for the basic sandalwood note [1]. Several synthetic procedures of its representative hydrocarbon counterparts 2 and 3 have been reported. *endo*-α-Bergamotene (2) has been pr epared by Gibson and Erman in 12 steps starting from β-pinene [2]. Corey, Cane and Libit have prepared *exo*-α-bergamotene (3) using a photochemical [2+2] cycloaddition of 1,5-d iene in 21 steps fro m geranyl acetate [3]. Larsen and Monti have prepared *endo*-α-bergamotene (2) and *exo*-isomer 3 using intramolecular ring closure for the formation of the cyclobutane ring in 13 steps [4]. Although the d irect construction of the acid-labile 2-methylbicyclo[3.1.1]hept-2-ene skeleton and the unambiguous stereocontrol of the quaternary C-6 carbon center h ave only been partially achieved by these earlier endeavors, these methods do not permit the accumulation of large amounts of mat erial owing to ma ny complicated steps and lo w overall yields.

Intramolecular [2+2] photocycloaddition is an important issue in organic s ynthesis directed towards target m olecules. The intramolecular [2+2] photocycloadditions between enone and olefin moieties have b een extensively studied in 2-, 3- and 4-substituted alkenylcyclohexenones and f ound numerous applications in synthesis [5]. To the best of ou r knowledge, intramolecular [2+2] photocycloaddition of 1,6 ,8-triene system was hitherto unknown. In this p aper we wish to r eport regiospecific intramolecular [2+2] photocycloadditions of two 1,6,8-trienes *i.e.* α,β,γ,δ-unsaturated ester and conjugated dienol, each of whi ch has a vin yl terminus. Irradiation of β-myrcene resulted in a non-regioselective mixture of several intramolecular products to afford β-pinene in a 22% yield as a result of [2+ 2] photocycloaddition between two double bonds among the three olefin moieties [6]. Our approach involv es the direct construction of the target ring molecule by the ir radiation of an acyclic precursor having a distal double bond and an α,β,γ,δ-unsaturated ester moiety which is expected having strong absorption in the ultraviolet region.

exo-(Z)-α-Bergamotol (1)   exo-α-Bergamotene (3)

endo-α-Bergamotene (2)   2-methylbicyclo-[3.1.1]hept-2-ene

We reported an *N*-ylide [2,3]- and [3,3] sigmatropic rearrangement that provides (*Z*)- or (*E*)-trisubstituted olefinic amines with hi gh stereoselectivity [7]. And the [2,3] sigmatropic rearr angement of ammonium ylides having an ethoxycarbonyl group at the α-position afforded exclusively (*E*)-amines [7b]. Thes e amines can b e converted to α,β,γ,δ-unsaturated esters via Cope elimination of the corresponding *N*-oxides.

As outlined in Scheme 1, hypochlorous acid, generated in situ from calcium hypochlorite and CO_2, reacted with (*R*)- (−)-linalool (4) to provide allylic chloride, which was treated with dimethylamine in aqueous EtOH at room temper ature to give the correspondin g allylamine 5 via regioselectiv e S_N2 reaction. Reaction of 5 with ethyl bromoacetate in EtOH pr ovided quaternary ammonium salt 6 in a quantitative yield. Treatment of 6 with NaOEt in EtOH at 0°C resulted in th e formation of ammonium ylide intermediate 7 followed by spontaneous [2,3]sigmatropic rearrangement to give (*E*)-amino ester 8 in 83% yield with 95% stereoselectivity. Furthermore, treatment of 6 with KO*t*-Bu in THF at −70°C afforded *E*-ester 8 in 72% yield with complete stereoselectivity.

Then amino ester 8 was treated with perac etic acid in CH_2Cl_2 at −60°C in the presence of N a_2CO_3 and the resulting mixture containing the amine oxide was stirred at room temperature for 30 min to giv e the desired (*E,E*)-α,β,γ,δ-unsaturated ester 9a via Cope elimination of amine oxide in 88% yield with complete

Scheme 1
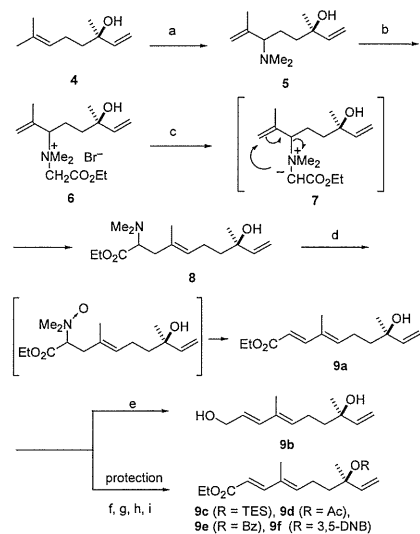
Conditions: (a) (i) Ca(OCl)$_2$, CO$_2$, CH$_2$Cl$_2$, rt, (ii) HNMe$_2$, EtOH, rt, 47% (2 steps),
(b) BrCH$_2$CO$_2$Et, MeOH , rt, quant., (c) KOt-Bu, THF, –70 °C, 72%,
(d) AcO$_2$H, Na$_2$CO$_3$, CH$_2$Cl$_2$, –60 °C, 88%, (e) AlCl$_3$ / LiAlH$_4$, ether, 0 °C, 56%,
(f) TESOTf, 2,6-lutidine, 84%, (g) AcCl, Et$_3$N, DMAP, quant., (h)BzCl, DMAP, quant.,
(i) 3,5-DNBCl, Et$_3$N, DMAP, 84%.

stereoselectivity. The ultraviolet absorption spectra analysis showed this unsaturated ester **9a** has large ε value (31500) at λ_{max} 267 nm. The subsequent reduction of **9a** was most effectively carried out with AlH$_3$ [8] prepared in situ from AlCl$_3$ and LiAlH$_4$ to give the corresponding unsaturated alcohol **9b** in 56% yield. The ultraviolet absorption spectra analysis showed this unsaturated alcohol **9b** has large ε value (24700) at λ_{max} 233 nm.

Regioselectivity of cross and/or parallel addition is a crucial point in [2+2] photocycloaddition chemistry. Srinivasan et al. suggested that the initial step, which gives a diradical, involves preferential formation of a five-membered ring ("rule of five") on intramolecular [2+2] photocycloaddition reactions of 1,6-heptadiene [9]. Similar results were obtained on intramolecular [2+2] photocycloaddition reaction of 3-methylene-1,5-hexadiene system [10].
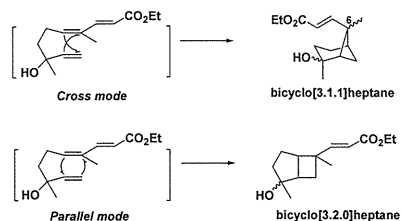
Irradiation of **9a** with the low pressure Hg lamp in each of hexane, c-hexane, diethyl ether or MeOH solution without a photosensitizer gave rise to an unidentified complex mixture of photoadducts. On the other hand, when **9a** was irradiated with the high pressure Hg lamp in benzene solution including 5-nitroacenaphthene (NAN) as a photosensitizer, a mixture of cross [2+2] adduct *endo*-**10a** and parallel photoadducts *endo*-**11a** and *exo*-**11a** was formed as a mixture that could not be separated. Then we confirmed these structures strictly by conversion of photoadducts into separable optically active compounds, *endo*-**12**, *endo*-**13** and *exo*-**13** [11] as shown in Scheme 2.

Scheme 2
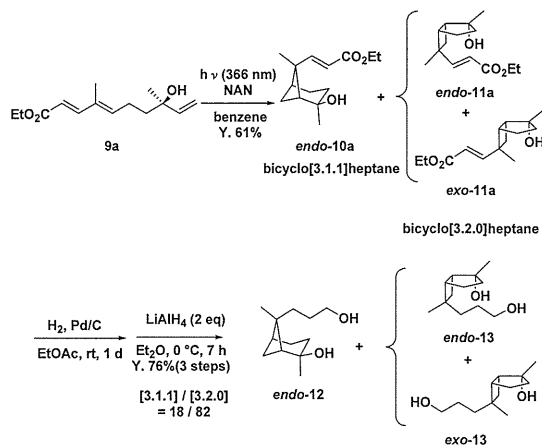
Thus, hydrogenation followed by reduction with LiAlH$_4$ afforded a cross [2+2] adduct (C-6 stereoisomer) *endo*-**12** and a mixture of two parallel photoadducts *endo*-**13** and *exo*-**13**as separable diols. The accurate ratio of *cross/parallel* was determined by capillary GC analysis. Thus triene **9a** gave a 18:82 mixture of two photoadducts which were identified as the cross adduct **10** and the parallel adduct **11** in 61% yield. This interesting result prompted us to investigate [2+2] photocycloaddition of triene **9c-f** which was supposed to have an inherent regioselectivity of *cross/parallel*-addition. Table 1 shows the photocycloaddition results.
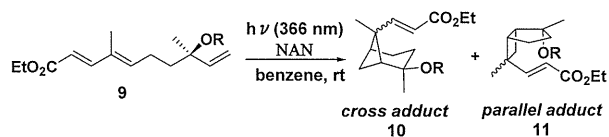
Table 1: Photocycloaddition reaction of triene **9**.

entry	9	R	Time(h)	Yield(%)	10/11[a]
1	9a	H	2	61	18/82
2	9c	TES	2	52	32/68
3	9d	Ac	3	79	30/70
4	9e	Bz	2	80	41/59
5	9f	3,5-(NO$_2$)$_2$C$_6$H$_3$CO	3	74	25/75

a) The ratio of **10/11** was determined by ^{1}H NMR and capillary GC analysis after conversion into diols12 and13.

The present photocycloaddition reaction depends on R substituents. When **9c** was irradiated in benzene, *cross*-selectivity increased going rise to a 32:68 mixture of two regioisomers, **10c** and **11c** in 52 % yield (Table 1, entry 2). Interestingly, when **9e** was irradiated in benzene solution, the yield of photoadducts **10** and **11** increased up to a 80 % (Table 1, entry 4). In addition, cross-selectivity increased up to 41:59.

endo-10   *exo*-10
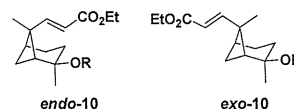
Table 2: Stereoselectivity on bicyclo[3.1.1]heptane ring system

entry	10	R	*endo/exo*[a]
1	10a	H	100/0
2	10c	TES	78/22
3	10d	Ac	100/0
4	10e	Bz	88/12
5	10f	3,5-(NO$_2$)$_2$C$_6$H$_3$CO	88/12

a) The ratio of *endo/exo* was determined by ^{1}H NMR.

It is interesting to note that wit h the *cross*-adduct **10a** or **10d**, the ratio of the two epimers at C-6 position on the bicy clo[3.1.1]ring has a value of 100:0 (Table 2, entr y 1, 3). A nd the prefer ence of *endo*-stereochemistry at C-6 bridged head was observed in other *cross*-adducts. So as to the stereoselectivity on bicyclo[3.2.0]heptane ring **11**, the stereoselectivity increased giving rise to a 87:13 mixture of two epimers *endo*-**11f** and *exo*-**11f** (Table 3, entry 5).

endo-11   *exo*-11
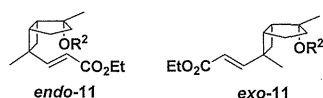
Table 3: Stereoselectivity on bicyclo[3.2.0]heptane ring system.

entry	11	R	*endo/exo*[a]
1	11a	H	51/49
2	11c	TES	53/47
3	11d	Ac	76/24
4	11e	Bz	77/23
5	11f	3,5-(NO$_2$)$_2$C$_6$H$_3$CO	87/13

a)   The ratio of *endo/exo* was determined by ^{1}H NMR.

We assume that the preference of *endo*-stereochemistry at C-6 bridged head is due to fast rotati on in the 1,4-biradical intermediate and the selectivity in the ring closure step reflects steric interactions in the transition state. The first bond is formed between the terminal double bond and excited diene. Rotation around the single bond in the most stab le 1,4-diradical intermediate was found to b e much faster than cyclization. Therefore *Z* or *E* trisubstituted olefin moiety of diene leads to the same product mixture. The conformational preference of TS-1 over TS-2 may result fr om the 1,3-diaxial repulsion B between the axial h ydrogen on cyclohex ane ring and the methyl substituent being larger than that of repulsion A between the axial hydrogen on cy clohexane ring and the 2-ethoxycarbonyl vinyl group as shown in Scheme 3.
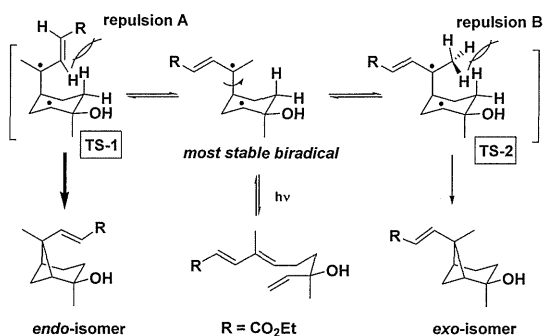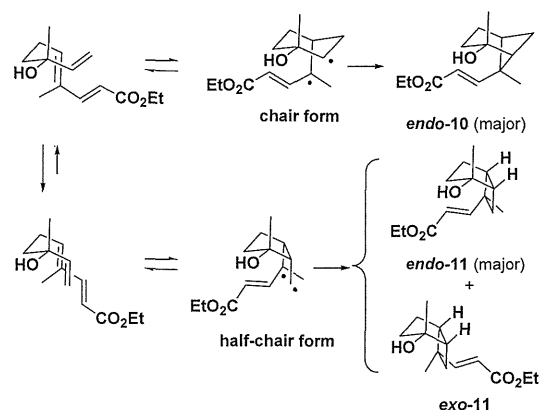

Scheme 3

Srinivasan suggested that the initial step, which gives a diradical, involves preferential formation of a five-membered ring ("rule of five") on intramolecular [2+2] photocycloaddition reactions of 1,6-heptadiene [9]. However, irr adiation of **9a** gave the cr oss photoadduct *endo*-**10** and some parallel adducts. This mode of the cross addition observed here is against the "rule of five" for intramolecular [2+2] photocycloadditions and points to the fact t hat no strict gen eralization can be made for such reactions [12] . We assumed the stable biradical of chair form may be attributed to the extra stabilization being called *the captodative effect* [13] which is synergistic stabilization of c arbon centered radicals by both an

electron-withdrawing (captive) and an electron-donating (dative) substituent as s hown in Schem e 4.Thus, it may be due to the stabilization of the r adical on tertiary carbon by both an ester vinylogue (captive) and a methyl (dative) substituent.

Scheme 4

On the other hand, using of **9b** instead of **9a**, no cycloadducts were observed on ex posure with the low pressure Hg lamp in each of hexane, diethyl ether, MeOH or benzene solutions. However, when **9b** was irradiated with the high pressure Hg lamp in acetone, two parallel adducts **14** originated through [2 +2] cycloaddition according to th e "rule of five " was obtained i n 39% yield. The structure of ph otoadducts **14** was confirmed b y the sequential hydrogenation to afford a 50:50 mixture of two 1,2-bridg ed cyclobutanes *endo*-**13** and *exo*-**13**.

[3.2.0]	[3.2.0]
endo-14	*exo*-14
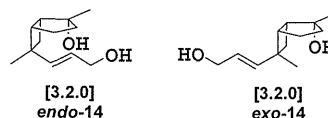
It is noteworth y that th e optically active 1,3-bridged cyclobutanes **10** of the bicy clo[3.1.1]heptane ring system and 1,2-bridged cyclobutanes **11** of the bicy clo[3.2.0]heptane ring s ystem were produced by UV irradiation of α,β,γ,δ-unsaturated esters **9a** and **9c-f**. These results suggest that a chirality on the C-8 atom can control the stereoselectivity of the cycloaddition reaction. The preference of *endo*-stereochemistry at C-6 bridged head was observed in *cross*-adducts **10**. On th e other hand, the regioselectivity was found to p roceed exclusively in the p arallel fashion when conjugated dienol **9b** was irradiated.

We expect that this methodology will be useful for the synthesis of a wide range of bergamotene family, and further work toward t his goal is in progress.

References

[1]   Brunke EJ. (**1983**) (-)-(Z)-α-*trans*-Bergamotol a newly isolated constituent of East Indian sandalwood oil of interest to perfumers. *Dragoco Report*, *2*, 27-32.

[2] Gibson TW, Erman WF. (**1969**) Syntheses of the (-)-α-and (+)-β-*cis*-bergamotenes. *Journal of the American Chemical Society*, *91*, 4771-4778.

[3] Corey EJ, Cane DE, Libit L.(**1971**) Synthesis of racemic α-*trans*- and β-*trans*-bergamotene.*Journal of the American Chemical Society*, *93*, 7016-7021.

[4] Larsen SD, Monti SA. (**1977**) Total synthesis of racemic α-*trans*- and α-*cis*-bergamotene and α-pinene. *Journal of the American Chemical Society*,*99*, 8015-8020.

[5] Reviews on intramolecular [2+2] photocycloadditions: (a) Crimmins MT. (**1988**) Synthetic applications of intramolecular enone-olefin photocycloadditions. *Chemical Reviews*, *88*, 1453-1473; (b) Crimmins MT. (**1991**) Photochemical cycloadditions. In *Comprehensive Organic Synthesis*.Vol. *5*, Paquette, LA.(Ed). Pergamon Press, London, UK. 123-150. Selectiveexamples of intramolecular [2+2] photocycloadditions: (c) BeckerD, Haddad N. (**1986**) About the stereochemistry of intramolecular [2+2] photocycloadditions. *Tetrahedron Letters*, *27*, 6393-6396; (d) Pirrung MC. (**1979**) Total synthesis of (±)-isocomene.*Journal of the American Chemical Society*, *101*, 7130-7131; (e) PirrungMC. (**1981**) Total synthesis of (±)-isocomene and related studies. *Journal of the American Chemical Society*, *103*, 82-87; (f) Cargill RL, Dalton JR, O'Connor S, Michels DG. (**1978**) Tricyclo[6.3.0.0^{1,6}]undecan-2-one and its isomerization to tricyclo[3.3.3.0]undecan-2-one. *Tetrahedron Letters*, 4465-4466; (g) CroftKD, Ghilsalberti EL, Jeffries PR, Stuart AD, Raston CL, White AR. (**1981**) Intramolecular [2+2] photoaddition of a 1,7-diene. *Journal of the Chemical Society, Perkin Transactions 2*, 1473-1480; (h) Mehta G, Acharyulu PVR. (**1994**) Terpenes to terpenes. Stereo- and enantio-selective synthesis of (+)-α-elemene and a short route to a versatile diquinanechiron. *Journal of Chemical Society,Chemical Communications*, 2759-2760.

[6] Crowley KJ. (**1965**) Photoisomerizations. VI. Cyclobutene formation and diene migration in simple 1,3-dienes. *Tetrahedron*, *21*, 1001-1014.

[7] (a) Honda K, Inoue S, Sato K. (**1990**) Highly stereocontrolled syntheses of isomeric pairs of di- and trisubstituted olefins through [2,3]sigmatropic rearrangement of allyldimethylammoniumm ethylides. *Journal of the American Chemical Society*, *112*, 1999-2001; (b) Honda K, Inoue S, Sato K. (**1992**) Stereoselective synthesis of trisubstituted *Z*- or *E*-olefins employing N-substituted β-methallyldimethylammonium ylides. *Journal of Organic Chemistry*, *57*, 428-429; (c) Honda K, Inoue S. (**1994**) Highly stereoselective synthesis of trisubstituted (*E*)-olefins using the base-induced [3,3]rearrangement of *N*-substituted β-methallyl-dimethylammonium salts in protic solvents. *Synlett*, 739-740; (d) Honda K, Tabuchi M, Inoue S. (**1996**) Stereocontrolled elongation of a functionalized isoprene unit on the *E* or *Z* terminal methyl of terpenoids via *N*-ylide rearrangement of the common ammonium salts. *Chemistry Letters*, 385-386; (e) Honda K, YoshiiI, Inoue S. (**1996**) Highly *Z* selective synthesis of functionalized monoterpenoids via N-ylide [2,3]sigmatropic rearrangement and its application to 13-*cis*-retinol. *Chemistry Letters*, 671-672; (f) Honda K, Igarashi D, Asami M, Inoue S. (**1998**) Stereoselective synthesis of oxygenated trisubstituted olefins using N-ylides [2,3]-rearrangement. *Synlett*, 685-687; (g) Honda K, Tabuchi M, Kurokawa H, Asami M, Inoue S. (**2002**) Stereocontrolled synthesis of acyclic terpenoids via *N*-ylide [2,3]rearrangement of ammonium salts with the stereodefined isoprene unit. *Journal of the Chemical Society, Perkin Transactions 1*, 1387-1396; (h) Honda K, Yasui H, Inoue S. (**2003**) Stereoselective synthesis of di- and tri-substituted aminoalkenes: tandem isomerization/ aza-Claisen rearrangement/hydride reduction sequence. *Synlett*, 2380-2382; (i) Honda K, Shibuya H, Yasui H, Hoshino Y, Inoue S. (**2008**) Copper-catalyzed intermolecular generation of ammonium ylides with subsequent [2,3]sigmatropic rearrangement: efficient synthesis of bifunctional homoallylamines. *Bulletin of the Chemical Society of Japan.*, *81*, 142-147; (j) Honda K, Shibuya H, Hoshino Y, Inoue S. (**2008**) Novel oxidative generation of ammonium ylides and subsequent silicon Polonovski reaction. *Chemistry Letters*, *37*, 442-443.

[8] Jorgenson MJ. (**1962**) Selective reductions with aluminum hydride. *Tetrahedron Letters*, 559-562.

[9] Srinivasan R, Carlough KH. (**1967**) Mercury(^{3}P$_1$) photosensitized internal cycloaddition reactions in 1,4-, 1,5-, and 1,6-dienes. *Journal of the American Chemical Society*, *89*, 4932-4936.

[10] LiuRSH, Hammond GS.(**1967**) Photosensitized internal addition of dienes to olefins. *Journal of the American Chemical Society*, *89*, 4936-4944.

[11] Isolated compounds were identified as follows:

*endo***-12:** Y. 16.1%, MP: 78.8°C.[α]$_D$^{20}: -24.8 (*c* 1.00, CHCl$_3$).Rf:0.40 (diethyl ether).IR (KBr):3286, 2948, 2863, 1462, 1374, 1197, 1182, 1112, 1075, 1057, 916 cm^{-1}.^{1}H NMR (400 MHz, CDCl$_3$): 1.13 (3H, s, H-11), 1.22 (3H, s, H-12), 1.16-1.47 (5H, m, H-9 , H-8, H$_{cis}$-7), 1.62-1.73 (4H, m, H-4, H$_{trans}$-7, H-3a),1.79-1.90 (1H, m, H-3e),2.36-2.45 (2H, m, H-5, H-1),3.62 (2H, t, *J* = 6.6 Hz, H-10).^{13}C NMR (100 MHz CDCl$_3$): 22.1(CH$_3$), 24.8(CH$_2$), 27.4(CH$_2$), 28.2(CH$_3$), 33.3(CH$_2$), 34.6(C), 35.6(CH$_2$), 39.9(CH$_2$), 44.8(CH), 47.7(CH), 63.6(CH$_2$), 81.5(C).

*exo***-13:** Y.6.5%, MP: 93.3°C.[α]$_D$^{20}:+25.2 (*c* 1.00, CHCl$_3$).Rf: 0.33(diethyl ether).IR (KBr):3244, 2946, 2864, 1453, 1373, 1170, 1066, 980 cm^{-1}. ^{1}H NMR (400 MHz, CDCl$_3$): 0.88 (3H, s, H-12), 1.20 (3H, s, H-8),1.44-1.72 (9H, m, H-3a, H-4, H$_{trans}$-7, H$_{cis}$-7, H-9 , H-10),1.90-1.97 (1H, m, H-3e),2.20 (1H, t, *J* = 7.2 Hz, H-5),2.32 (1H, dd, *J* = 15.5 Hz, 6.8 Hz ,H-1),3.65 (2H, t, *J* = 6.1 Hz, H-11).^{13}C NMR (100 MHz CDCl$_3$): 20.6(CH$_3$), 24.4(CH$_2$), 27.4(CH$_3$), 27.6(CH$_2$), 32.1(CH$_2$), 35.0(C), 39.0(CH$_2$), 39.9(CH$_2$), 42.6(CH), 44.4(CH), 63.4(CH$_2$), 79.0(C).

*endo***-13:** Y.54.1%, [α]$_D$^{20}: +23.0 (*c* 1.00, CHCl$_3$). Rf: 0.28 (diethyl ether). IR (neat):3336, 2948, 2865, 1455, 1372, 1169, 1143, 1058, 977, 916, 917 cm^{-1}.^{1}H NMR (400 MHz, CDCl$_3$):1.06 (3H, s, H-12), 1.14 (3H, s, H-8),1.18-1.60 (9H, m, H-4, H-3a, H$_{trans}$-7, H$_{cis}$-7, H-9, H-8),1.81-1.89 (1H, m, H-3e),2.12 (1H, t, *J* = 7.6 Hz, H-5),2.30 (1H, dd, *J* = 15.2 Hz, 7.2 Hz ,H-1),3.64 (2H, t, *J* = 6.4 Hz, H-11).^{13}C NMR (100 MHz CDCl$_3$): 24.1(CH$_2$), 27.2(CH$_2$), 27.3(CH$_3$), 28.4(CH$_3$), 32.5(CH$_2$), 32.6(CH$_2$), 34.8(C), 39.1(CH$_2$), 42.2(CH), 46.2(CH), 63.3(CH$_2$), 81.5(C).

[12] WolffS, AgostaW. (**1983**) Regiochemical control in intramolecular photochemical reactions of 1,5-hexadien-3-ones and 1-acyl-1,5-hexadienes. *Journal of the American Chemical Society*, *105*, 1292-1299.

[13] Reviews: (a) Viehe HG, Merenyi R, Stella L, JanousekZ. (**1979**) New synthetic method. 32. Capto-dative substitution. 5. Capto-dative substituent effects in syntheses with radicals and radicophiles. *Angewandte Chemie*, *91*, 982-997; (b) Viehe HG, Janousek Z, Merenyi R, Stella L. (**1985**) The captodative effect. *Accounts of Chemical Research*, *18*, 148-154; (c) Viehe HG, Merenyi R, JanousekZ.(**1988**) Captodative substituent effect. Part 45. Captodative substituent effects in radical chemistry. *Pure and Applied Chemistry*, *60*, 1635-1644; (d) Viehe HG, Janousek Z, Merenyi R. (**1989**) Captodative substituent effects. 44. Captodative substituent effect in synthesis. In *NATO ASI Series, Series C: Mathematical and Physical Sciences (Free Radicals in Synthesis and Biology)*, Minisci F. (Ed). Kluwer Academic Publishers, Dordrecht, 1-26; (e) Sustmann R, Korth H-G. (**1990**) The captodative effect. *Advances in Physical Organic Chemistry*, *26*, 131-178.

Review/Account

Natural Product Communications

2012

Volume 7, Number 4

Contents

Continued inside backcover

Vanadium-Catalyzed Oxidation of *tert*-Butyl *N*-Hydroxycarbamate to *tert*-Butyl Nitrosoformate and Its Diels–Alder Reaction with Simple and Functionalized Dienes

Yujiro Hoshino,* Kenzo Suzuki, Kiyoshi Honda

Graduate School of Environment and Information Sciences, Yokohama National University, 79-7 Tokiwadai, Hodogaya-ku, Yokohama 240-8501, Japan
Fax +81(45)3394434; E-mail: yhoshino@ynu.ac.jp

Abstract: A general and efficient vanadium-catalyzed oxidation of *tert*-butyl *N*-hydroxycarbamate to *tert*-butyl nitrosoformate using alkyl hydroperoxides as terminal oxidants has been developed. The intermediate nitroso compound was trapped by in situ Diels–Alder reaction with simple and functionalized dienes, providing general access to a variety of functionalized 3,6-dihydro-2*H*-1,2-oxazines.

Key words: nitroso Diels–Alder reaction, catalysis, oxidation, functionalized dienes, vanadium catalyst

The nitroso Diels–Alder (NDA) reaction is an intriguing method for synthetic organic chemists due to the selective 1,4-incorporation of amino and hydroxy functionalities into 1,3-dienes in a single step.[1] Among nitroso compounds nitrosocarbonyl compounds, RCONO, are well-known to be very powerful dienophiles[2] and are typically generated in situ by the stoichiometric oxidation of hydroxamic acids, using organic or inorganic periodates,[1a,3] Dess–Martin periodinane,[4] oxalyl chloride,[5] *N*-bromosuccinimide,[6] silver oxide,[6] lead oxide,[6] or by thermally liberation from their NDA adducts with 9,10-dimethylanthracene in refluxing solvent.[1] In view of green chemistry, catalytic reactions and safer reagents are preferable. Therefore, metal-catalyzed oxidations involving peroxides as the terminal oxidants have recently emerged for the generation of nitrosocarbonyl compounds.[7] Late transition metals, especially Ru and Cu, have been extensively examined as a catalyst for these reactions.

Acylnitroso Diels–Alder reactions with 1,3-dienes having functional groups would directly furnish functionalized 3,6-dihydro-1,2-oxazines, which possess a great potential for the synthesis of nitrogen-containing natural products.[2b,e,8] However, since the first reports by Whiting,[7a] and Iwasa and Nishiyama,[7b] only simple 1,3-dienes have been examined in the metal-catalyzed oxidation of hydroxamic acids to nitroso compounds and their Diels–Alder reactions.[9] Herein we describe the vanadium-catalyzed oxidation of *tert*-butyl *N*-hydroxycarbamate using alkyl hydroperoxides as terminal oxidants and in situ Diels–Alder trapping of nitrosoformate with simple and functionalized dienes (Scheme 1). In a single step this

potentially allows access to polyfunctionalized 1,2-oxazines which are versatile intermediates for preparing nitrogen-containing bioactive compounds.
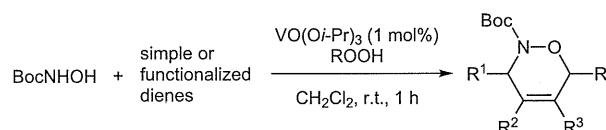
Scheme 1

Our studies began with the reaction of *tert*-butyl *N*-hydroxycarbamate (BocNHOH) with hexa-2,4-dien-1-ol (**1a**) in the presence of cumyl hydroperoxide (CHP) as a terminal oxidant. In the absence of any catalyst, no Diels–Alder adduct was detected and BocNHOH was quantitatively recovered (Table 1, entry 1). On the other hand, when a catalytic amount (1 mol%) of VO(O*i*-Pr)₃ was added to the reaction mixture (at –20 °C for 1 h), the [4+2] cycloadducts **2a** and **3a** were obtained in 65% yield (Table 1, entry 2).[10] Increasing the amount of BocNHOH and CHP (1.5 and 2.0 equiv) improved the yields of the Diels–Alder adducts (Table 1, entries 3 and 4). When commercial-grade or water-saturated dichloromethane was used as the solvent, the yield of adducts was slightly decreased (72% yield). It is noteworthy that raising the temperature from –20 °C to room temperature resulted in a complete conversion of dienol **1a**, affording the Diels–Alder adduct in quantitative yield (Table 1, entry 5). It is well known that epoxidation of allylic alcohols smoothly proceeds under the above reaction conditions except in the presence of an excess amount of hydroxamic acids.[11] Indeed, ¹H NMR analysis of the reaction mixture, which was obtained from the vanadium-catalyzed reaction of hexadienol **1a** with CHP at room temperature for one hour, showed the exclusive formation of the corresponding epoxide (see Supporting Information). On the other hand, in the presence of two equivalents of BocNHOH the cycloadducts were quantitatively obtained with no observation of oxidized byproducts such as epoxides and aldehydes.[12] Thus, these results imply a formation of stable hydroxamate complexes from the vanadium ion and hydroxamic acid, which substantially forbids the concurrent coordination of dienol **1a** and oxidant to vanadium, leading to the inhibition of epoxidation of dienol **1a**. Interestingly, compared to the literature result (80% yield, regioisomeric ratio of **2a**/**3a** = 67:33) in which tetrabutylammonium periodate

was used as an stoichiometric oxidant, our oxidation system gave the adducts in quantitative yield with slightly higher regioselectivity (99% yield, **2a/3a** = 72:28).[13] These results suggest that some involvement of concurrent coordination of the nitrosoformate and hexadienol **1a** to vanadium could exist in the Diels–Alder reaction, which would control their orientation in the bond-forming step and would enhance the regioselectivity. Even 0.1 mol% of VO(Oi-Pr)$_3$ gave the desired Diels–Alder adduct in good yield (Table 1, entry 6). While the use of 1.1 equivalents of BocNHOH and two equivalents of oxidant gave a satisfactory result (r.t., 1 h, 80% yield, Table 1, entry 7), the reverse case (2 equiv of BocNHOH and 1 equiv of oxidant, Table 1, entry 8) led to complete conversion of the starting material to give the desired product in high yield (1 h, 99% yield). Other nonpolar solvents, for example toluene and cyclopentylmethylether (CPME), were also used as a solvent (Table 1, entries 9 and 10). The reaction catalyzed by titanium complex, instead of vanadium catalyst, also proceeded in satisfactory yield but needed a much longer reaction time (12 h, Table 1, entry 11). The reaction using *tert*-butyl hydroperoxide (TBHP, 5.5 M in decane) as an oxidant gave almost the same result with CHP (Table 1, entry 12). Hydrogen peroxide (30%) was not an effective oxidant for this reaction (Table 1, entry 13).

With optimized reaction conditions [VO(Oi-Pr)$_3$ (1 mol%), oxidant (1 equiv), BocNHOH (2 equiv), r.t., 1 h] in our hands, various simple or functionalized dienes were subjected to these optimized conditions.[14] Our oxidation system proved to be general for a variety of simple dienes (Table 2, entries 1–5). Cyclic and acyclic conjugated dienes afforded the desired 3,6-dihydro-1,2-oxazines in good yields (Table 2, entries 1–3). The reaction with 9,10-dimethylanthrathene, which is frequently used to mask nitrosocarbonyl compounds,[1] gave the NDA adduct **2e** in moderate yields (Table 2, entry 4). The reaction with 2-substituted diene **1f** afforded the desired 1,2-oxadines in a 1:1 ratio of regioisomers **2f** and **3f** (Table 2, entry 5), which was consistent with the literature result.[15] The 1:1 mixture of regioisomers was also obtained from myrcene (**1g**), having a trisubstituted double bond, in low yield due to the ability to polymerize under the workup conditions (Table 2, entry 6).

A single isomeric adduct was obtained in moderate yield from the reaction with sorbic acid as a functionalized diene (Table 2, entry 7). The reaction with sorbic acid deriv-

Table 1 Optimization of Vanadium-Catalyzed Oxidation of BocNHOH Using CHP and in situ Diels–Alder Reaction with (*E,E*)-Hexa-2,4-dien-1-ol (**1a**)
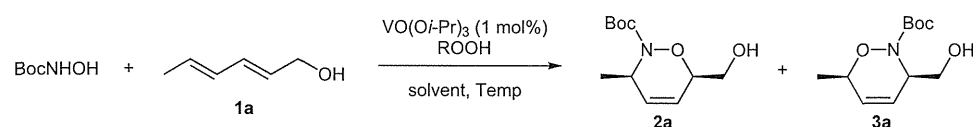
Entry	BocNHOH (equiv)	ROOH (equiv)	Solvent	Temp (°C)	Time (h)	Yield (%)[a]	Ratio of **2a/3a**[b]
1[c]	2	CHP (2)	CH$_2$Cl$_2$	–20	1	0	–
2	1	CHP (1)	CH$_2$Cl$_2$	–20	1	65	83:17
3	1.5	CHP (1.5)	CH$_2$Cl$_2$	–20	1	94	79:21
4	2	CHP (2)	CH$_2$Cl$_2$	–20	1	95	77:23
5	2	CHP (2)	CH$_2$Cl$_2$	r.t.	0.5	99	72:28
6[d]	2	CHP (2)	CH$_2$Cl$_2$	r.t.	1	71	74:26
7	1.1	CHP (2)	CH$_2$Cl$_2$	r.t.	1	80	78:22
8	2	CHP (1)	CH$_2$Cl$_2$	r.t.	1	99	77:23
9	2	CHP (2)	toluene	r.t.	0.5	99	79:21
10	2	CHP (2)	CPME	r.t.	2	80	71:29
11[e]	2	CHP (2)	CH$_2$Cl$_2$	r.t.	12	85	78:22
12	2	TBHP (2)	CH$_2$Cl$_2$	r.t.	1	91	77:23
13	2	H$_2$O$_2$ (2)	CH$_2$Cl$_2$	r.t.	2	27[f]	80:20[g]

[a] Isolated yield of **2a** and **3a** after silica gel chromatography.
[b] The ratio is based on the isolated yields of the regioisomers.
[c] The reaction was carried out in the absence of vanadium catalyst. BocNHOH was recovered quantitatively.
[d] VO(Oi-Pr)$_3$ (0.1 mol%) was used.
[e] Ti(Oi-Pr)$_4$ (1 mol%) was used.
[f] The adduct **2a** was obtained as a mixture with BocNHOH. The yield of **2a** was calculated on the basis of ^{1}H NMR analysis of the mixture.
[g] The ratio was determined by ^{1}H NMR spectroscopy.

atives **1i–l** also gave exclusively the 1,2-oxadines **2i–l** as single stereoisomers (Table 2, entries 8–11). Interestingly, the Diels–Alder reaction with silyl-protected dienoate ester **1k** gave a lower yield compared to unmasked hydroxy dienoate ester **1j**, implying a steric repulsion between the triisopropylsilyl group and the *tert*-butoxycarbonyl group. Weinreb amide **1l** is also a good substrate for this reaction, giving the desired adduct **2l** in a good yield (Table 2, entry 11). When 2-silyloxy-substituted cyclohexadiene **1m** was used as a functionalized diene, Diels–Alder adduct **2m** was obtained in low yield (Table 2, entry 12). This adduct

is likely to desilylate on the silica gel during column chromatography, giving α-hydroxyaminocyclohexenone.

In summary we have demonstrated the vanadium-catalyzed oxidation of *tert*-butyl *N*-hydroxycarbamate using alkyl hydroperoxides and its Diels–Alder reaction with simple and functionalized dienes. This useful reaction proceeds rapidly under mild conditions (1 mol% catalyst loading, r.t., 1 h), leading to good yields of functionalized 1,2-oxadines, which are considered promising synthetic intermediates for highly functionalized compounds. Synthetic studies to access useful natural products are currently under way and will be reported in due course.

Table 2 Acylnitroso Diels–Alder Reaction with Various Simple and Functionalized Dienes
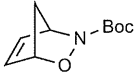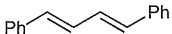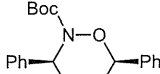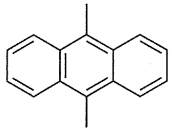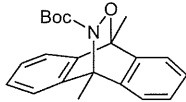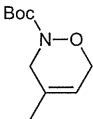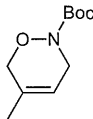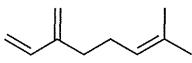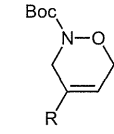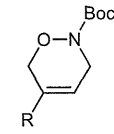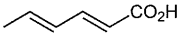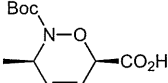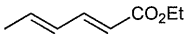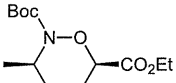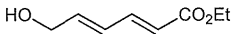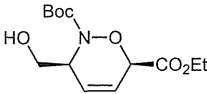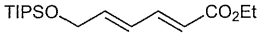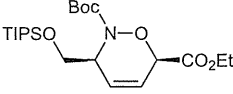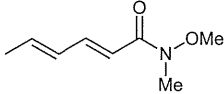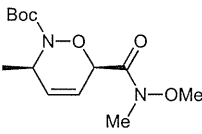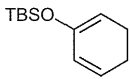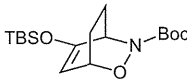
Entry	Diene	Oxidant	Products	Yield (%)[a]
1[b]	**1b**	CHP	**2b**	62
2[c]	**1c**	CHP	**2c**	86
3	**1d**	CHP	**2d**	77
4	**1e**	TBHP	**2e**	40
5	**1f**	TBHP	**2f** **3f**	46[d]
6	**1g**	CHP	R = Me₂C=CHCH₂CH₂ **2g** **3g**	20[d]
7	**1h**	CHP	**2h**	44
8	**1i**	TBHP	**2i**	70

Table 2 Acylnitroso Diels–Alder Reaction with Various Simple and Functionalized Dienes (continued)

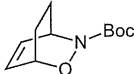| Entry	Diene	Oxidant	Products	Yield (%)[a]
9	HO~~~CO₂Et **1j**	CHP	**2j** HO, Boc N–O, CO₂Et	62
10	TIPSO~~~CO₂Et **1k**	TBHP	**2k** TIPSO, Boc N–O, CO₂Et	20
11	(diene **1l**)	TBHP	**2l** Boc, N–O, C(=O)N(Me)OMe	79
12	TBSO (diene **1m**)	CHP	**2m** TBSO, N–Boc, O (bicyclic)	13[e]

[a] Isolated yield.
[b] The reaction temperature was –20 °C.
[c] Toluene was used as solvent.
[d] The ratio of regioisomers was 1:1.
[e] N-Boc-6-hydroxyamino-2-hexenone was produced in 24% yield.

Acknowledgment

Supporting Information for this article is available online at http://www.thieme-connect.com/ejournals/toc/synlett.

References and Notes

(1) (a) Kirby, G. W. *Chem. Soc. Rev.* **1977**, *6*, 1. (b) Yamamoto, Y.; Yamamoto, H. *Eur. J. Org. Chem.* **2006**, 2031.

(2) (a) Kirby, G. W.; Sweeny, J. G. *J. Chem. Soc., Chem. Commun.* **1973**, 704. (b) Bodnar, B. S.; Miller, M. J. *Angew. Chem. Int. Ed.* **2011**, *50*, 5630. (c) Li, F.; Yang, B.; Miller, M. J.; Zajicek, J.; Noll, B. C.; Möllmann, U.; Dahse, H.-M.; Miller, P. A. *Org. Lett.* **2007**, *9*, 2923. (d) Vogt, P. F.; Miller, M. J. *Tetrahedron* **1998**, *54*, 1317. (e) Iwasa, S.; Fakhruddin, A.; Nishiyama, H. *Mini-Rev. Org. Chem.* **2005**, *2*, 157.

(3) Kirby, G. W.; Sweeny, J. G. *J. Chem. Soc., Perkin Trans. 1* **1981**, 3250.

(4) Jenkins, N. E.; Ware, R. W. Jr.; Atkinson, R. N.; King, S. B. *Synth. Commun.* **2000**, *30*, 947.

(5) Martin, S. F.; Hartmann, M.; Josey, J. A. *Tetrahedron Lett.* **1992**, *33*, 3583.

(6) Dao, L. H.; Dust, J. M.; Mackay, D.; Watson, K. N. *Can. J. Chem.* **1979**, *57*, 1712.

(7) (a) Flower, K. R.; Lightfoot, A. P.; Wan, H.; Whiting, A. *Chem. Commun.* **2001**, 1812. (b) Iwasa, S.; Tajima, K.;

Tsushima, S.; Nishiyama, H. *Tetrahedron Lett.* **2001**, *42*, 5897. (c) Chaiyaveij, D.; Cleary, L.; Batsanov, A. S.; Marder, T. B.; Shea, K. J.; Whiting, A. *Org. Lett.* **2011**, *13*, 3442. (d) Howard, J. A. K.; Ilyashenko, G.; Sparkes, H. A.; Whiting, A.; Wright, A. R. *Adv. Synth. Catal.* **2008**, *350*, 869. (e) Howard, J. A. K.; Ilyashenko, G.; Sparkes, H. A.; Whiting, A. *Dalton Trans.* **2007**, 2108. (f) Adamo, M. F. A.; Bruschi, S. *J. Org. Chem.* **2007**, *72*, 2666. (g) Chow, C. P.; Shea, K. J. *J. Am. Chem. Soc.* **2005**, *127*, 3678. (h) Pulacchini, S.; Sibbons, K. F.; Shastri, K.; Motevalli, M.; Watkinson, M.; Wan, H.; Whiting, A.; Lightfoot, A. P. *Dalton Trans.* **2003**, 2043. (i) Flower, K. R.; Lightfoot, A. P.; Wan, H.; Whiting, A. *J. Chem. Soc., Perkin Trans. 1* **2002**, 2058. (j) Iwasa, S.; Fakhruddin, A.; Tsukamoto, Y.; Kameyama, M.; Nishiyama, H. *Tetrahedron Lett.* **2002**, *43*, 6159.

(8) (a) Streith, J.; Defoin, A. *Synthesis* **1994**, 1107. (b) Kibayashi, C.; Aoyagi, S. *Synlett* **1995**, 873.

(9) Recently, copper-catalyzed aerobic oxidation of N-hydroxycarbamates to nitrosoformates and their nitroso ene reaction with functionalized olefins was reported, see: Frazier, C. P.; Engelking, J. R.; Read de Alaniz, J. *J. Am. Chem. Soc.* **2011**, *133*, 10430.

(10) **Typical Procedure for the Vanadium-Catalyzed Oxidation of *tert*-Butyl N-Hydroxycarbamate and in situ Diels–Alder Reaction with (E,E)-Hexa-2,4-dien-1-ol (1a)**
To a solution of *tert*-butyl N-hydroxycarbamate (0.564 g, 4.1 mmol), (E,E)-hexa-2,4-dien-1-ol (0.246 mL, 2.1 mmol), and VO(Oi-Pr)₃ (5.0 μL, 0.021 mmol) in CH₂Cl₂ (4.2 mL) was added 80% CHP (0.39 mL, 2.1 mmol) at ambient temperature. After stirring for 1 h, H₂O (2 mL) was added to the mixture. A sat. Na₂SO₃ solution was slowly added to the resulting mixture. After stirring for 1 h, the reaction mixture was transferred to a separatory funnel, and the aqueous

phase was extracted with CH_2Cl_2 (5 × 5 mL). The combined organic phases were washed with brine, dried over anhyd Na_2SO_4, filtered, and concentrated under reduced pressure. Flash chromatographic purification (eluent: hexane–Et_2O = 3:1 to 2:1) of the residue provided **2a** and **3a** (0.480 g, 99%) as a mixture of two regioisomers. The mixture was separated by column chromatography on silica gel (hexane–EtOAc = 9:1) to give pure **2a** and **3a**. The structure was deduced from two-dimensional NMR spectroscopy (HMBC and HMQC).[13]

(3R*,6R*)-N-tert-Butoxycarbonyl-6-hydroxymethyl-3-methyl-3,6-dihydro-2H-1,2-oxazine (2a)[13]
TLC: R_f = 0.26 (hexane–EtOAc = 1:1). IR (neat): 3407, 2978, 1698, 1369, 1169, 1119, 1066 cm^{-1}. ^{1}H NMR (300 MHz, CDCl$_3$): δ = 1.32 (d, J = 9.0 Hz, 3 H), 1.47–1.49 (m, 1 H), 1.50 (s, 9 H), 3.67 (dd, J = 6.6, 12.6 Hz, 1 H), 3.77 (dd, J = 3.0, 12.3 Hz, 1 H), 4.41–4.46 (m, 1 H), 4.64–4.68 (m, 1 H), 5.69 (dt, J = 10.2, 1.8 Hz, 1 H), 5.92 (ddd, J = 10.2, 4.5, 2.4 Hz, 1 H).

(3S*,6S*)-N-tert-Butoxycarbonyl-3-hydroxymethyl-6-methyl-3,6-dihydro-2H-1,2-oxazine (3a)[13]
TLC: R_f = 0.38 (hexane–EtOAc = 1:1). IR (neat): 3445, 2979, 1704, 1369, 1166, 1113, 1088 cm^{-1}. ^{1}H NMR (300 MHz, CDCl$_3$): δ = 1.26 (d, J = 6.6 Hz, 3 H), 1.50 (s, 9 H), 1.65 (s, 1 H), 3.72–3.77 (m, 2 H), 4.47–4.52 (m, 1 H), 4.65–4.68 (m, 1 H), 5.78 (ddd, J = 10.2, 4.2, 2.1 Hz, 1 H), 5.85 (td, J = 1.5, 10.2 Hz, 1 H).

(11) (a) Sharpless, K. B.; Michaelson, R. C. *J. Am. Chem. Soc.* **1973**, *95*, 6136. (b) Sharpless, K. B.; Verhoeven, T. R. *Aldrichimica Acta* **1979**, *12*, 63. (c) Michaelson, R. C.; Palermo, R. E.; Sharpless, K. B. *J. Am. Chem. Soc.* **1977**, *96*, 1990.

(12) Zeng, W.; Ballard, T. E.; Melander, C. *Tetrahedron Lett.* **2006**, *47*, 5923.

(13) Calvet, G.; Blanchard, N.; Kouklovsky, C. *Synthesis* **2005**, 3346.

(14) *N-tert*-Butoxycarbonyl-2-oxa-3-azabicyclo[2.2.1]hept-5-ene (2b)[16]
TLC: R_f = 0.33 (hexane–Et$_2$O = 1:2). IR (neat): 2978, 1739, 1702, 1165 cm^{-1}. ^{1}H NMR (300 MHz, CDCl$_3$): δ = 1.47 (s, 9 H), 1.73 (d, J = 8.6 Hz, 1 H), 1.99 (td, J = 2.4, 8.6 Hz, 1 H), 4.98 (br s, 1 H), 5.21 (br s, 1 H), 6.40–6.42 (m, 2 H).
N-tert-Butoxycarbonyl-2-oxa-3-azabicyclo[2.2.2]oct-5-ene (2c)[16]
TLC: R_f = 0.51 (hexane–EtOAc = 3:1). IR (neat): 2976, 2936, 1736, 1695, 1158, 1073 cm^{-1}. ^{1}H NMR (300 MHz, CDCl$_3$): δ = 1.27–1.54 (m, 2 H), 1.47 (s, 9 H), 2.06–2.23 (m, 2 H), 4.73–4.75 (m, 2 H), 6.50–6.59 (m, 2 H).
(3S*,6R*)-N-tert-Butoxycarbonyl-3,6-diphenyl-3,6-dihydro-2H-1,2-oxazine (2d)
TLC: R_f = 0.39 (hexane–EtOAc = 5:1). IR (neat): 2978, 1700, 1392, 1368, 1166, 1094, 699 cm^{-1}. ^{1}H NMR (300 MHz, CDCl$_3$): δ = 1.49 (s, 9 H), 5.56 (br s, 1 H), 5.59 (br s, 1 H), 6.09 (d, J = 10.5 Hz, 1 H), 6.16 (ddd, J = 10.8, 4.5, 2.1 Hz, 1 H), 7.26–7.53 (m, 10 H). ^{13}C NMR (75 MHz, CDCl$_3$): δ = 28.4, 79.0, 81.7, 126.4, 127.7, 127.8, 128.2, 128.5, 128.7, 129.0, 137.2, 139.2, 154.2.
N-tert-Butoxycarbonyl-1,8-dimethyl-15-oxa-16-azatetracyclo[6.6.2.0^{2,7}.0^{9,14}]hexadec-2,4,6,9,11,13-hexaene (2e)[4]
Mp 106–109 °C. TLC: R_f = 0.33 (hexane–EtOAc = 5:1). IR (KBr): 2981, 1707, 1460, 1288, 1159, 748 cm^{-1}. ^{1}H NMR (300 MHz, CDCl$_3$): δ = 1.21 (s, 9 H), 2.23 (s, 3 H), 2.56 (s, 3 H), 7.23–7.27 (m, 4 H), 7.34–7.38 (m, 2 H), 7.43–7.46 (m, 2 H).

A 1:1 Mixture of N-tert-Butoxycarbonyl-4-methyl-3,6-dihydro-2H-1,2-oxazine (2f) and N-tert-Butoxycarbonyl-5-methyl-3,6-dihydro-2H-1,2-oxazine (3f)[13]
TLC: R_f = 0.66 (hexane–EtOAc = 6:1). IR (neat): 2978, 2933, 1705, 1683, 1392, 1368, 1243, 1166, 1102 cm^{-1}. ^{1}H NMR (300 MHz, CDCl$_3$): δ = 1.50 [s, 9 H, 3 × CH$_3$ (3f)], 1.51 (s, 9 H, 3 × CH$_3$), 1.67 [br s, 3 H, CH$_3$-5 (3f)], 1.74 (br s, 3 H, CH$_3$-4), 3.94 (br s, 2 H, H-3), 4.02–4.05 [m, 2 H, H-3 (3f)], 4.26 [br s, 2 H, H-6 (3f)], 4.35–4.38 (m, 2 H, H-6), 5.51–5.55 [m, 1 H + 1 H, overlapped with H-5 and H-4 (3f)].

A 1:1 Mixture of N-tert-Butoxycarbonyl-4-(4-methylpent-3-enyl)-3,6-dihydro-2H-1,2-oxazine (2g) and N-tert-Butoxycarbonyl-5-(4-methylpent-3-enyl)-3,6-dihydro-2H-1,2-oxazine (3g)
TLC: R_f = 0.64 (hexane–EtOAc = 6:1). IR (neat): 2976, 2929, 1727, 1703, 1366, 1162, 1092 cm^{-1}. ^{1}H NMR (300 MHz, CDCl$_3$): δ = 1.50 (s, 9 H + 9 H), 1.60 (s, 3 H + 3 H), 1.69 (s, 3 H + 3 H), 1.98–2.12 (m, 4 H + 4 H), 3.97 (br s, 2 H), 4.05 (br s, 2 H), 4.29 (br s, 2 H), 4.39 (br s, 2 H), 5.05–5.12 (m, 1 H + 1 H), 5.52 (br s, 1 H + 1 H). ^{13}C NMR (75 MHz, CDCl$_3$): δ = 17.7, 25.6, 25.8, 25.9, 28.3, 32.7, 33.9, 44.9, 47.6, 68.0, 70.4, 81.4, 116.0, 117.6, 123.3, 132.3, 134.2, 135.5, 155.0.

N-tert-Butoxycarbonyl-6-carboxy-3-methyl-3,6-dihydro-2H-1,2-oxazine (2h)
TLC: R_f = 0.68 (MeOH). IR (KBr): 2977, 1748, 1686, 1370, 1156, 1121 cm^{-1}. ^{1}H NMR (300 MHz, CDCl$_3$): δ = 1.36 (d, J = 6.6 Hz, 3 H), 1.51 (s, 9 H), 4.43 (br s, 1 H), 5.16 (s, 1 H), 5.93–6.03 (m, 2 H). ^{13}C NMR (75 MHz, CDCl$_3$): δ = 17.9, 28.3, 50.8, 75.9, 82.8, 121.9, 130.6 154.5, 170.5.

N-tert-Butoxycarbonyl-6-ethoxycarbonyl-3-methyl-3,6-dihydro-2H-1,2-oxazine (2i)[17]
TLC: R_f = 0.63 (hexane–EtOAc = 6:1). IR (neat): 2980, 1760, 1738, 1705, 1369, 1312, 1196, 1169, 1076, 1032, 716 cm^{-1}. ^{1}H NMR (300 MHz, CDCl$_3$): δ = 1.32 (t, J = 7.1 Hz, 3 H), 1.36 (d, J = 6.8 Hz, 3 H), 1.50 (s, 9 H), 4.27 (q, J = 7.2 Hz, 2 H), 4.46–4.48 (m, 1 H), 5.14–5.16 (m, 1 H), 5.90 (td, J = 1.3, 10.4 Hz, 1 H), 5.98 (ddd, J = 10.2, 4.3, 2.5 Hz, 1 H).

N-tert-Butoxycarbonyl-6-methoxycarbonyl-3-hydroxymethyl-3,6-dihydro-2H-1,2-oxazine (2j)
TLC: R_f = 0.24 (hexane–EtOAc = 1:1). IR (neat): 3446, 2979, 1737, 1707, 1475, 1251, 1157, 1071, 1024 cm^{-1}. ^{1}H NMR (300 MHz, CDCl$_3$): δ = 1.50 (s, 9 H), 3.73–3.88 (m, 2 H), 3.82 (s, 3 H), 4.51–4.55 (m, 1 H), 5.52 (s, 1 H), 6.00 (ddd, J = 10.2, 3.9, 2.1 Hz, 1 H), 6.06 (td, J = 1.5, 10.5 Hz, 1 H). ^{13}C NMR (75 MHz, CDCl$_3$): δ = 28.2, 52.8, 56.6, 63.0, 74.3, 82.8, 124.3, 125.7, 155, 167.6.

N-tert-Butoxycarbonyl-3-[(triisopropylsilyloxy)methyl]-6-methoxycarbonyl-3,6-dihydro-2H-1,2-oxazine (2k)
TLC: R_f = 0.77 (hexane–EtOAc = 1:1). IR (neat): 2943, 2867, 1766, 1740, 1710, 1367, 1109, 881, 681 cm^{-1}. ^{1}H NMR (300 MHz, CDCl$_3$): δ = 1.02–1.13 (m, 3 H), 1.06 (d, J = 3.9 Hz, 18 H), 1.49 (s, 9 H), 3.80 (s, 3 H), 3.82 (dd, J = 9.6, 7.8 Hz, 1 H), 3.97 (dd, J = 9.3, 6.6 Hz, 1 H), 4.48–4.49 (m, 1 H), 5.16–5.19 (m, 1 H), 6.02 (td, J = 1.8, 10.2 Hz, 1 H), 6.16 (ddd, J = 10.2, 4.2, 2.7 Hz, 1 H). ^{13}C NMR (75 MHz, CDCl$_3$): δ = 11.9, 17.9, 28.3, 52.6, 55.8, 64.1, 74.7, 82.1, 123.2, 127.3, 154.1, 167.9.

N-tert-Butoxycarbonyl-6-(N'-methoxy-N'-methylcarbamoyl)-3-methyl-3,6-dihydro-2H-1,2-oxazine (2l)
TLC: R_f = 0.25 (hexane–Et$_2$O = 1:2). IR (neat): 3592, 2979, 2934, 1681, 1369, 1172, 992, 714 cm^{-1}. ^{1}H NMR (300 MHz, CDCl$_3$): δ = 1.37 (d, J = 6.6 Hz, 3 H), 1.51 (s, 9 H), 3.24 (br s, 3 H), 3.84 (s, 3 H), 4.45–4.47 (m, 1 H), 5.53 (br s, 1 H), 5.86 (br s, 1 H), 5.99 (ddd, J = 10.5, 5.1, 2.4 Hz, 1 H). ^{13}C

NMR (75 MHz, CDCl$_3$): δ = 17.9, 28.4, 32.4, 50.7, 62.2, 74.3, 81.7, 122.3, 130.0, 154.2.

N-*tert*-Butoxycarbonyl-3-[(*tert*-butyldimethylsilyloxy)-methyl]-6-methoxycarbonyl-3,6-dihydro-2*H*-1,2-oxazine (2m)

TLC: R_f = 0.66 (hexane–EtOAc = 1:1). IR (neat): 2954, 2930, 2857, 1766, 1741, 1710, 1253, 1106, 834, 777 cm^{-1}.
^{1}H NMR (300 MHz, CDCl$_3$): δ = 0.07 (s, 6 H), 0.89 (s, 9 H), 1.49 (s, 9 H), 3.73 (dd, *J* = 9.9, 7.2 Hz, 1 H), 3.81 (s, 3 H), 3.88 (dd, *J* = 10.2, 7.2 Hz, 1 H), 4.46 (br s, 1 H), 5.16–5.19 (m, 1 H), 6.01 (td, *J* = 1.5, 10.2 Hz, 1 H), 6.11 (ddd, *J* = 10.5, 4.2, 2.7 Hz, 1 H). ^{13}C NMR (75 MHz, CDCl$_3$): δ = –5.3, –5.3, 18.2, 25.6, 25.8, 28.3, 52.6, 55.8, 63.6, 74.7, 82.1, 123.5, 127.0, 154.2, 167.8.

(15) Adamo, M. F. A.; Bruschi, S. *J. Org. Chem.* **2007**, *72*, 2666.
(16) Zhang, D.; Süling, C.; Miller, M. J. *J. Org. Chem.* **1998**, *63*, 885.
(17) Bollans, L.; Bacsa, J.; Iggo, J. A.; Morris, G. A.; Stachulski, A. V. *Org. Biomol. Chem.* **2009**, *7*, 4531.
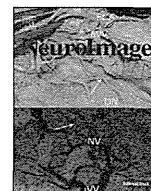
Systematic changes to the apparent diffusion tensor of in vivo rat brain measured with an oscillating-gradient spin-echo sequence

Jeff Kershaw [a,b,*], Christoph Leuze [c], Ichio Aoki [a], Takayuki Obata [d], Iwao Kanno [a], Hiroshi Ito [a], Yuki Yamaguchi [b], Hiroshi Handa [b]

[a] Molecular Imaging Center, National Institute of Radiological Sciences, Chiba, Japan
[b] School of Bioscience and Biotechnology, Tokyo Institute of Technology, Yokohama, Japan
[c] Department of Neurophysics, Max Planck Institute for Human Cognitive and Brain Sciences, Leipzig, Germany
[d] Research Centre for Charged Particle Therapy, National Institute of Radiological Sciences, Chiba, Japan

ARTICLE INFO

ABSTRACT

As the oscillating gradient spin-echo sequence has shown promise as a means to probe tissue microstructure, it was applied here to diffusion-tensor imaging of in vivo rat brain. The apparent diffusion tensor (ADT) was estimated for motion-probing gradient (MPG) frequencies in the range 33.3–133.3 Hz, and regions-of-interest (ROIs) in the corpus callosum (CC), visual cortex (VC), cerebellar white matter (CBWM) and cerebellar grey matter (CBGM) were selected for detailed analysis. There were substantial, approximately linear changes to the ADT with increasing MPG frequency for all four ROIs. All ROIs showed clear increases in mean diffusivity. CBWM had a substantial decrease in fractional anisotropy, whereas the CC and VC had minor increases of the same parameter. All eigenvalues of the ADT tended to increase with frequency for the CBWM, CBGM and VC, but only the principal eigenvalue increased strongly for the CC. On the other hand, there was no evidence that the orientation of the principal eigenvector varied systematically with MPG frequency for any of the ROIs. The relationship between the behaviour of the eigenvalues and the behaviours of the mean diffusivity and fractional anisotropy is investigated in detail. Pixelwise linear fits to the MD from individual animals found elevated changes across the cerebellum. The data acquired for this work encompassed a range of effective diffusion-times from 7.5 ms down to 1.875 ms, and some ideas on how the results might be used to extract quantitative information about brain tissue microstructure are discussed.

© 2012 Elsevier Inc. All rights reserved.

Introduction

Many studies with diffusion-weighted MRI have indicated that manipulating the parameters of the motion-probing gradients (MPGs) offers a noninvasive means to probe in vivo tissue microstructure. One parameter routinely modified to alter image contrast is the orientation of the MPGs. Cycling the MPG direction around a hemisphere while preserving other parameters is used in diffusion-tensor MRI (DTI) (Basser et al., 1994) and other techniques like q-ball (Tuch, 2004) and HARDI (Tuch et al., 2002) to investigate tissue anisotropy. Another parameter with the potential to modify image contrast is the diffusion-time. Modulating the diffusion-time is often

cited as a means to investigate restricted or hindered diffusion in complex media, but it is widely neglected in clinical situations because evidence for distinct, unequivocal contrast changes in vivo is sparse.

Most studies investigating the effects of varying diffusion-time on image contrast in diffusion-weighted MRI have been performed with conventional pulsed-gradient spin-echo (PGSE) and pulsed-gradient stimulated-echo (PGStE) sequences. Using these sequences, changes to the signal with decreasing diffusion-time have been found in a variety of biological systems, including in vitro cell cultures (Pilatus et al., 1997), ex vivo rat brain (Assaf and Cohen, 1998) and in vivo radiation-induced tumors (Helmer et al., 1995). In vivo experiments on normal tissue have also been performed, but, with two exceptions, the studies were limited to diffusion-times of 8 ms or longer and no significant signal changes were observed (Clark et al., 2001; Le Bihan et al., 1993; Moonen et al., 1991; Niendorf et al., 1996; van Gelderen et al., 1994). One of the exceptions reported changes for diffusion-times in the range 33.3–793.3 ms (Horsfield et al., 1996). However, as the b-value of a sequence is not independent of the diffusion-time and no precautions seem to have been taken to keep the b-value constant, other researchers have questioned whether

the observed signal changes can be unambiguously attributed to a diffusion-time dependent effect (Clark et al., 2001; Does et al., 2003). In the second exception, a bipolar MPG was placed in only the first half of the echo-time so that diffusion-times as low as 1.6 ms were possible (Niendorf et al., 1994). At a constant b-value of 210 s/mm^2, the signal was found to decrease as the diffusion-time was reduced from 5.9 to 3.4 ms, suggesting that diffusion-time related contrast changes can be observed in vivo if the diffusion-time is less than around 5 ms, something that is difficult to achieve with standard PGSE and PGStE sequences.

As an alternative to PGSE and PGStE, the oscillating-gradient spin-echo (OGSE) sequence has been proposed as a means to reach diffusion-times of less than 5 ms (Gross and Kosfeld, 1969; Schachter et al., 2000). While OGSE was originally implemented with sinusoidal MPGs, more recent versions employ an apodised cosinusoidal shape (Does et al., 2003; Parsons et al., 2003). For an apodised cosinusoidal MPG of dominant frequency f, an effective diffusion-time of $1/4f$ can be improvised by equating the b-values calculated for the PGSE and OGSE sequences. Under this prescription, OGSE has been used to observe diffusion-time dependent signal changes and subsequently estimate the surface-to-volume ratio in systems of packed beads (Parsons et al., 2003; Parsons et al., 2006). It has also been employed to investigate intracellular restriction effects in in vitro cell preparations (Colvin et al., 2011; Xu et al., 2011), and, most importantly, demonstrate diffusion-time dependent signal changes in normal and diseased rat brain in vivo (Colvin et al., 2008; Does et al., 2003). Even though it has recently been pointed out that the effective diffusion-time construct only applies over a limited range of frequencies (Novikov and Kiselev, 2011), it has nonetheless been firmly established that OGSE provides a unique image contrast and is therefore a promising technique for probing in vivo tissue microstructure.

In most previous studies with the OGSE sequence, little consideration has been given to the consequences of varying MPG orientation. If frequency-dependent effects are observable when the MPG is applied in one direction, it follows that combining orientation and frequency modulated experiments may provide an interesting new method to investigate tissue properties. A similar idea has already been considered for the PGSE and PGStE sequences, but in terms of the diffusion-time. For example, the diffusion-time dependence of the mean diffusivity (MD), which is the trace of the apparent diffusion tensor (ADT) divided by 3, has been investigated with those sequences in several studies (e.g. Le Bihan et al., 1993; Horsfield et al., 1996). In those cases, however, data was only acquired in the three principal gradient directions so that the full ADT and apparent anisotropy could not be estimated. The only study where the dependence of the full ADT on diffusion-time has been investigated was that by Clark et al. (2001), who found no changes to the ADT, possibly because the shortest diffusion-time employed in the study (8 ms) was too long. With the introduction of the OGSE sequence, it seems possible that alterations to the ADT with diffusion-time may be observable if the correspondence between MPG frequency and effective diffusion-time is utilised. The only earlier applications of this idea were to ex vivo monkey brain (Xu et al., 2010) and ex vivo mouse brain (Aggarwal et al., 2012). The goal of this study was to combine OGSE with DTI-like acquisition and analysis protocols to investigate the MPG frequency dependence of the ADT in rat brain in vivo. An interpretation of the results in terms of restricted diffusion and the effective diffusion-time is also considered. Some of the results have been previously presented in abstract form (Kershaw et al., 2010, 2011).

Materials and methods

All experiments were approved by the Animal Welfare Committee of the National Institute of Radiological Sciences, Chiba, Japan.

Eleven male Sprague–Dawley rats (age 7–9 weeks, weight 200–300 g) were anaesthetised with isoflurane (4% for induction and 2% during the imaging experiments) and fixed in a MRI compatible cradle with bite and ear bars. The cradle was inserted into the bore of the magnet and then rotated so that the animal was upside-down to minimise the effects of respiratory motion. Rectal temperature was maintained at around 37 °C with heated air throughout the experiment. All MRI data were acquired on a 7 T MRI system (Magnet: Kobelco, Japan; Console: Bruker Avance I, Germany) equipped with an actively-screened gradient system (Bruker BGA12). A volume coil (diameter 72 mm, Bruker) was used for transmission and a 2-channel phased-array surface coil (13 mm × 15 mm, Rapid Biomedical, Germany) was used for signal reception. The latter coil was positioned over the head of the animal centred near the interaural plane to maximise the signal received from both the cerebellum and caudal end of the cerebrum.

Data acquisition was performed with a four-shot SE-EPI sequence modified to have one apodised cosinusoidal MPG waveform placed on either side of the π-refocussing pulse (Does et al., 2003; Parsons et al., 2003; Colvin et al., 2008). The sequence was set up so that the user first selects the duration T of the MPG lobes, which determines the base frequency $f = 1/T$, and then the desired harmonics of f and the maximum b-value are entered. The b-value as a function of frequency is $(\gamma G_k / 2\pi f_k)^2 (1 - 1/8k)T$, where $f_k = kf$ is the frequency of the kth harmonic and G_k is the peak amplitude of the applied MPG (Does et al., 2003; Parsons et al., 2003). The code automatically set G_k so that b remains constant with increasing k. The code was also configured so that $b = 0$ data was acquired when a value of zero was included in the list of harmonics. After choosing the harmonics, the user selected the number of directions in which to apply the oscillating MPGs. Unit vectors defining the directions were either entered by hand or read in from a set of prepared files. Acquisition of the data for a single experiment then proceeded in two major loops: the outer loop cycled through the MPG directions and the inner loop cycled through the list of selected harmonics.

A 1 mm thick sagittal slice set at 1–1.5 mm away from the midplane of the brain was selected for imaging. This orientation and position ensured that the slice passed through both the cerebellum and the thickest part of the corpus callosum. Three experiments, distinguished by different sets of MPG parameters, were performed on each animal (see Table 1). Note that the selected harmonics were limited to those where G_k did not exceed 91% of the maximum available gradient (404 mT/m). Each experiment acquired images for 78 evenly distributed MPG directions. Other common imaging parameters were TR = 3 s, matrix size = 128 × 128, FOV = 25.6 mm × 25.6 mm, and spatial resolution = 0.2 mm × 0.2 mm × 1 mm. T_2-weighted anatomical images of the same slice were also acquired with a standard multi-SE sequence (TR = 3 s, 14 echoes, TE = 10–140 ms).

The data was reconstructed and analysed offline using purpose-written Matlab code. No spatial or temporal smoothing was applied at any point during the analysis. The six independent elements of the ADT were estimated pixel-by-pixel for each harmonic from each experiment on each animal using a standard DTI analysis technique (Basser et al., 1994). Partially guided by the MD and fractional anisotropy (FA) maps calculated from the lowest frequency data of the type A experiments listed in Table 1, regions-of-interest (ROIs) were drawn by hand on the anatomical images of each animal. The same ROIs

Table 1
Oscillating MPG parameters for the three experiments performed on each animal.

Expt	TE (ms)	T (ms)	Max b (s/mm^2)	k	f_k (Hz)
A	71	26	1000	1, 2	38.5, 76.9
B	71	26	450	1, 2, 3	38.5, 76.9, 115.4
C	79	30	400	1, 2, 3, 4	33.3, 66.6, 100, 133.3

were used for all experiments on a particular animal. After averaging across the ROIs and collecting the data from all animals, the frequency dependence of the MD, FA and eigenvalues (EVs) of the ADT were evaluated. In addition, possible alteration to the orientation of the ADT with MPG frequency was investigated by grouping the principal eigenvectors of the ADT from all experiments by frequency, and then applying a parametric analysis-of-variance-like hypothesis test devised for groups of unit vectors on a sphere (Schwartzman et al., 2005; Mardia and Jupp, 2000).

All parameter estimation was performed with conventional multivariate linear least-squares fitting. Uncertainty in the parameter estimates was determined by bootstrapping the original data set (Efron and Tibshirani, 1994). Apart from the dependence on MPG frequency, it is possible that animal differences and the effects of other imaging parameters, such as the maximum *b*-value or TE, might also affect the ADT. Even so, multiple harmonics were acquired during each experiment and analysis of the data found that the trend with frequency was similar across experiments and animals. For that reason, the uncertainty of the estimates was evaluated by randomly sampling from the pool of experiments rather than the full data set as independent points. In practice, this means that when a data point from a particular experiment was randomly sampled, all data from that experiment was also included. In this way the variation contributed by differences between animals or imaging parameters is accounted for and the true uncertainty associated with the frequency dependence can come to the fore.

Results

Water and asparagus samples

To verify that the OGSE DTI protocol produces sensible results in a model system, it was first applied to pure water and asparagus samples (Fig. 1). Consistent with expectations, the MD (Fig. 1a), FA (Fig. 1b) and EVs (Fig. 1c) of the ADT estimated from the water data are insensitive to MPG frequency in the range 15–170 Hz. Regardless of frequency the

MD had a value of around $2\,\mu m^2/ms$, which is close to the value expected for the diffusion coefficient of water at room temperature. Similarly, the FA was estimated to be approximately 0.04 for all frequencies. The near isotropy of the water sample is reinforced by the similarity of the three EVs across frequencies.

In contrast, the results from the asparagus data show that the ADT is dependent on MPG frequency in the presence of microstructure. The MD of the asparagus increases with MPG frequency towards the water value (Fig. 1a). At the same time, the FA decreases from ≈ 0.26 at 25 Hz to ≈ 0.1 at 150 Hz (Fig. 1b). The EVs are plotted in Fig. 1d. At the lowest MPG frequency, the relatively large difference between the largest EV (blue) and each of the two smaller EVs (green and red) is consistent with the expected anisotropy of water motion in asparagus. However, while the largest EV remains approximately constant, the smaller EVs increase with MPG frequency and thus the apparent anisotropy decreases accordingly.

In vivo rat studies

Figs. 2a and b are the MD and FA maps, respectively, from a typical rat. The results are similar to what might be observed with standard PGSE or PGStE sequences. Arrows on the FA image point to the higher FA of the cerebellar white matter (CBWM) and the splenium of the corpus callosum (CC). Taking these two areas as ROIs with high apparent anisotropy, and adding cerebellar grey matter (CBGM) and visual cortex (VC) ROIs as examples of tissue with lower anisotropy (Fig. 2c), it is desired to analyse the frequency dependence of the ADT in those areas. Note that the $b=0$ images typically had signal-to-noise ratios of ~15–20 in the visual cortex and ~10–15 for the cerebellar ROIs.

The mean and standard deviation of the MD across experiments are plotted against MPG frequency in Fig. 3. Even though the MDs calculated for different experiments and animals may have varied by around 10–30%, the MD from any experiment tended to show the same trend with frequency for all ROIs. From inspection it appears that there is an upward trend of the MD with frequency for the
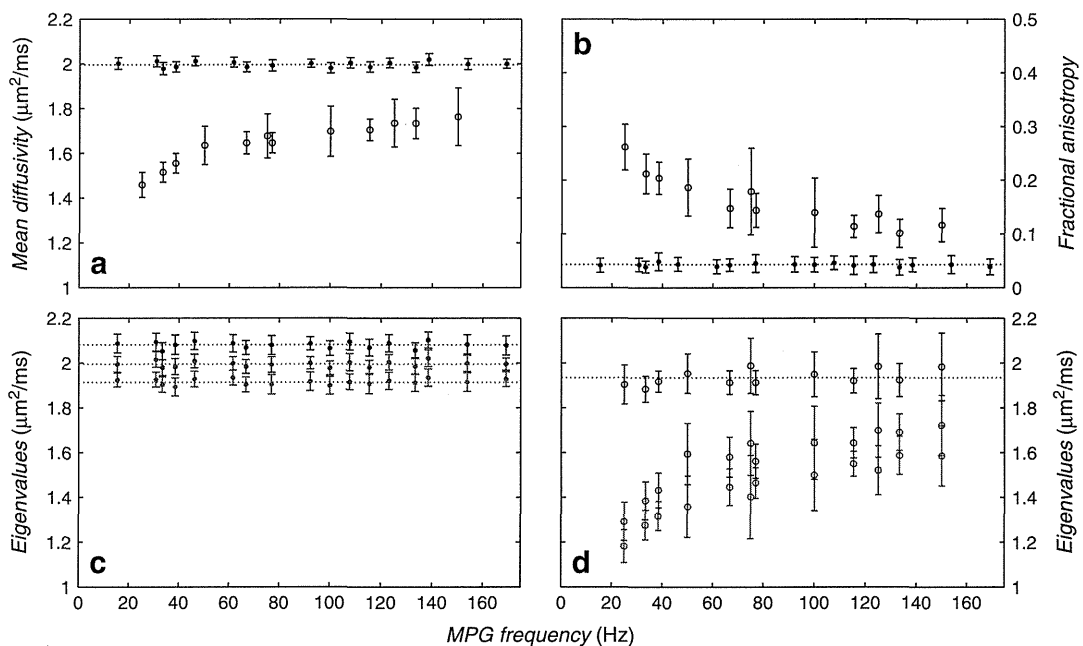
Fig. 1. The OGSE DTI protocol applied to pure water (closed circles) and asparagus (open circles) samples. (a) Mean diffusivity. (b) Fractional anisotropy. (c) Eigenvalues for the water data. (d) Eigenvalues for the asparagus data. The water data is insensitive to MPG frequency while the signal from the asparagus demonstrates a clear dependence on frequency. The error bars correspond to the standard deviation across the selected ROIs.
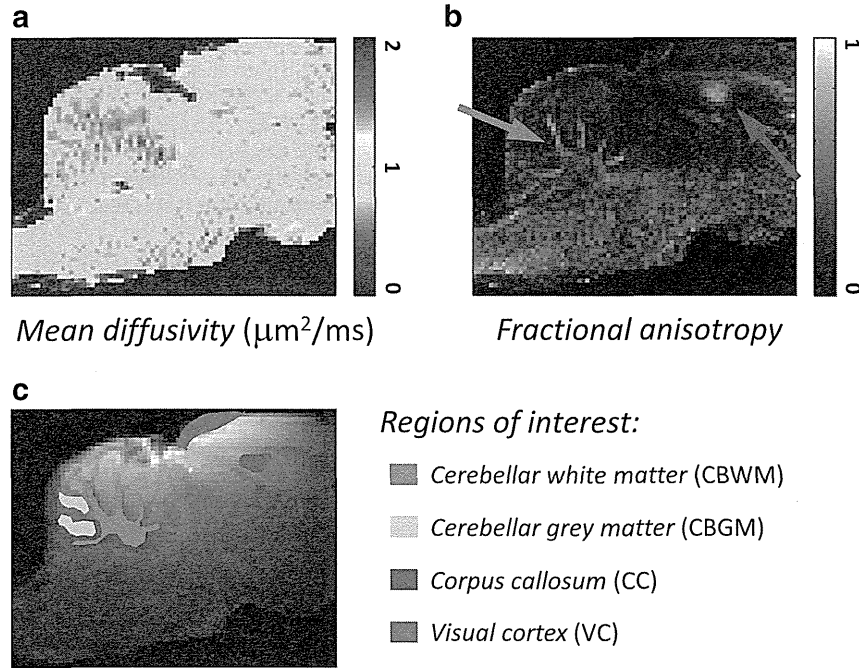
Fig. 2. OGSE DTI (a) MD and (b) FA maps from a typical rat. Note the arrows pointing to the higher FAs of the cerebellar white matter (CBWM) and splenium of the corpus callosum (CC) in (b). (c) The frequency dependence of the ADT was analysed in detail for regions-of-interest in the CBWM, cerebellar grey matter (CBGM), CC and visual cortex (VC).

CBWM and CBGM, and perhaps for the other ROIs as well. As the increase appears to be approximately linear over the range of frequencies used, the change in MD was characterised by fitting a straight line $\alpha_{MD}f + \beta_{MD}$ to the data with linear least-squares. If there is a significant change to the MD with frequency then the slope α_{MD} of the fitted line should be significantly different from zero. The fitted lines are plotted on top of the data in Fig. 3 and the estimates for α_{MD} are presented in Fig. 4a. The estimates for all four ROIs are positive.

Moreover, the 95% confidence intervals obtained from bootstrapping the data do not overlap zero. Therefore, it is possible to conclude that the MD increases significantly for each ROI, although more so for the CBWM and CBGM ROIs than for the CC and VC ROIs.

Fig. 5 similarly presents the mean and standard deviation of the FA across experiments plotted against MPG frequency. The behaviour of this data with MPG frequency was also characterised by a fit to a straight line. The fitted lines are plotted on top of the data in Fig. 5
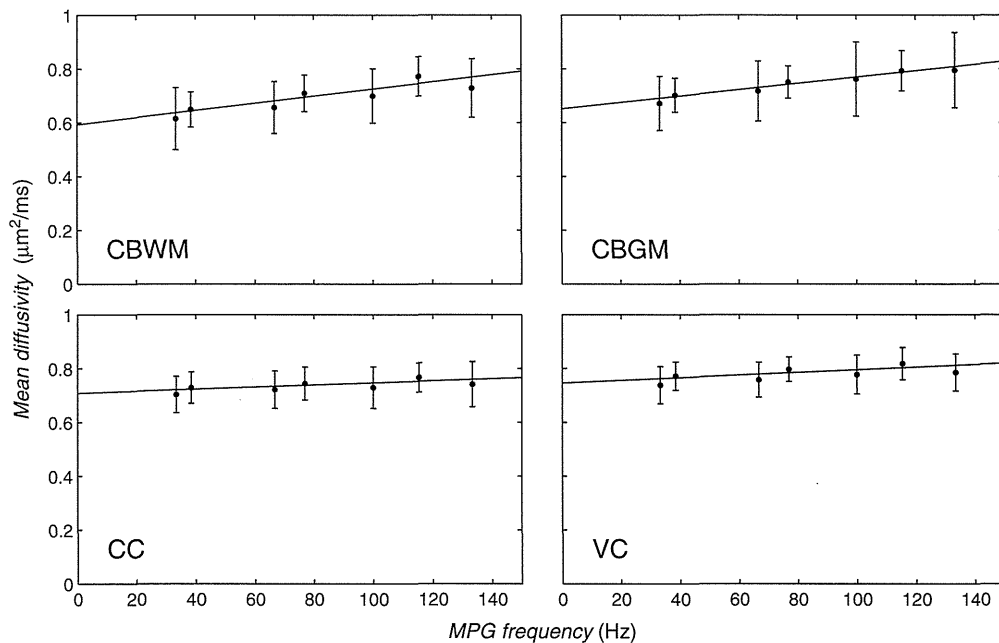

Fig. 3. MD plotted against MPG frequency for all four ROIs. The error bars represent the standard deviation of the MD across animals and experiments at the same frequency. The CBWM and CBGM appear to have a clear upward trend with increasing frequency. The solid lines are straight line fits to the data, with the estimates and uncertainty of the slopes shown in Fig. 4a.
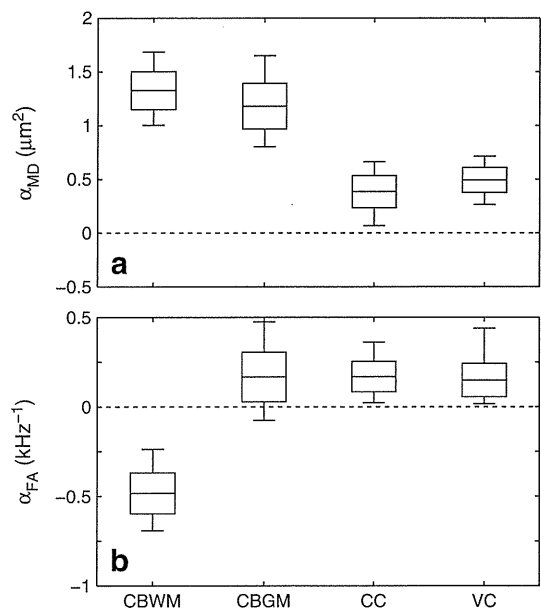
Fig. 4. Box-whisker plots of (a) α_{MD} and (b) α_{FA} estimated from straight-line fits with respect to MPG frequency for all ROIs. The boxes represent the standard deviation of the estimates and the thinner bars are the 95% confidence intervals.

and the estimates for the slope, α_{FA}, are presented in Fig. 4b. The estimate for the CBWM ROI is significantly less than zero, indicating a substantial decrease of FA with frequency in this ROI. While the 95% confidence interval of the CBGM indicates that the FA was independent of frequency for that ROI, the intervals for the CC and VC narrowly exclude zero, suggesting a minor increase of the apparent anisotropy in those ROIs.

The EVs of the ADT are presented in Fig. 6. Note that there is a more pronounced separation between the largest and two smaller EVs of the CBWM and CC than there is for the CBGM and VC. This difference is the source of the higher apparent anisotropies of the CBWM

and CC. Changes to the EVs with MPG frequency were again characterised with a straight line fit and the estimates for the slope $(\alpha_{\lambda_i}, i = 1,2,3)$ are shown in Fig. 7. The estimates of the α_{λ_i} for the CBWM and CBGM ROIs are significantly greater than zero, which means that all three EVs in those areas are increasing with MPG frequency. The same is true for the EVs of the VC ROI, although the rates of increase are less than those for the CBWM and CBGM and the 95% confidence interval of the smallest EV only narrowly excludes zero. For the CC ROI, while the largest EV increases significantly with frequency, both the second and third EVs are relatively unaffected in comparison.

Fig. 8 provides a simple graphical illustration of the dependence of the principal eigenvectors on frequency for all ROIs. Note that the CC has a very tight formation that makes it difficult to distinguish individual points, while the spread of the CBWM and CBGM eigenvectors is less dense but still well localised. The compact nature of these distributions suggests that they might be described by bipolar Watson distributions (Mardia and Jupp, 2000). In contrast, the VC eigenvectors are better described by a girdle-like Watson distribution because the data is spread along a circumference of the sphere. Grouping the eigenvectors by frequency and taking the null hypothesis to be the assumption that the mean directions of the groups are equal, the consistency in orientation of the principal eigenvectors was evaluated by applying a hypothesis test based on a Watson distribution of the appropriate type for each ROI. As presented in Table 2, all ROIs have *P*-values greater that 0.5 so there is no strong basis to reject the null hypothesis. In support of this, the black solid lines on Fig. 8 indicate that the mean directions of the ROIs did not evolve with frequency in any obvious systematic way.

Discussion

There were substantial, approximately linear changes to the rat ADT with increasing MPG frequency for all four in vivo ROIs. The ADT in the CBWM demonstrated strong increases to the EVs and MD, as well as a significant decrease in the FA. Both the CBGM and VC had significant increases in the EVs and MD, but there was no or only a minor change to the FA. The situation was more complex for
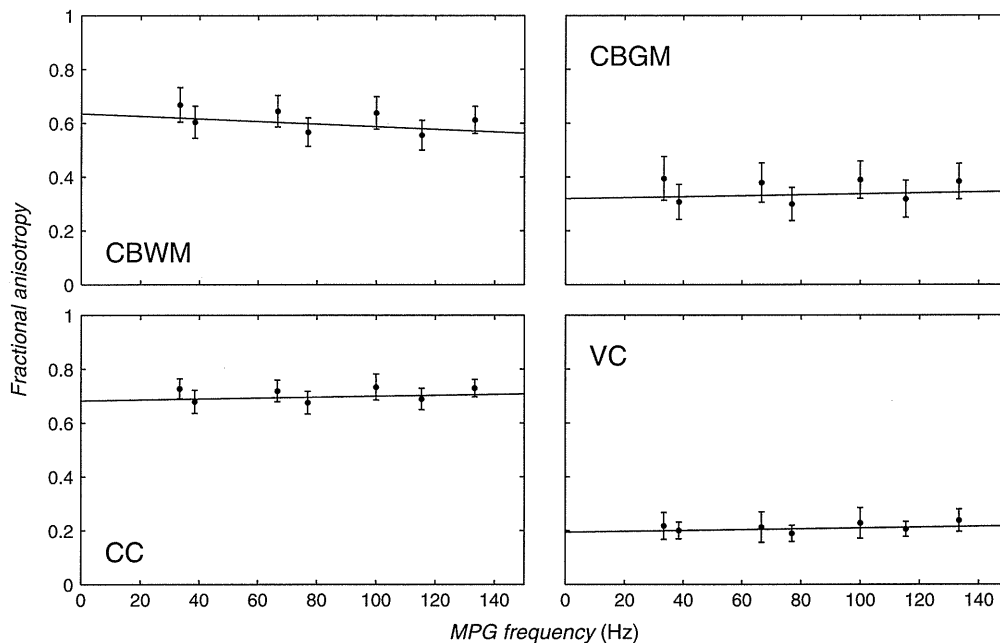

Fig. 5. FA plotted against MPG frequency for all four ROIs. The error bars represent the standard deviation of the FA across animals and experiments at the same frequency. The CBWM has a clear downward trend with increasing frequency. The solid lines are straight line fits to the data, with the estimates and uncertainty of the slopes shown in Fig. 4b.